Importance of composition and hygroscopicity of BC particles to the effect of BC mitigation on cloud properties: Application to California conditions

Ranjit Bahadur,[1] Lynn M. Russell,[1] Mark Z. Jacobson,[2] Kimberly Prather,[1,3] Athanasios Nenes,[4] Peter Adams,[5] and John H. Seinfeld[6]

[1]   Black carbon (BC) has many effects on climate including the direct effect on atmospheric absorption, indirect and semi-direct effects on clouds, snow effects, and others. While most of these are positive (warming), the first indirect effect is negative and quantifying its magnitude in addition to other BC feedbacks is important for supporting policies that mitigate BC. We use the detailed aerosol chemistry parcel model of Russell and Seinfeld (1998), observationally constrained by initial measured aerosol concentrations from five California sites, to provide simulated cloud drop number (CDN) concentrations against which two GCM calculations – one run at the global scale and one nested from the global-to-regional scale are compared. The GCM results reflect the combined effects of their emission inventories, advection schemes, and cloud parameterizations. BC-type particles contributed between 16 and 20% of cloud droplets at all sites even in the presence of more hygroscopic particles. While this chemically detailed parcel model result is based on simplified cloud dynamics and does not consider semi-direct or cloud absorption effects, the cloud drop number concentrations are similar to the simulations of both Chen et al. (2010b) and Jacobson (2010) for the average cloud conditions in California. Reducing BC particle concentration by 50% decreased the cloud droplet concentration by between 6% and 9% resulting in the formation of fewer, larger cloud droplets that correspond to a lower cloud albedo. This trend is similar to Chen et al. (2010b) and Jacobson (2010) when BC particles were modeled as hygroscopic. This reduction in CDN in California due to the decrease in activated BC particles supports the concern raised by Chen et al. (2010a) that the cloud albedo effect of BC particles has a cooling effect that partially offsets the direct forcing reduction if other warming effects of BC on clouds are unchanged. These results suggests that for regions like the California sites studied here, where BC mitigation targets fossil fuel sources, a critical aspect of the modeled reduction is the chemical composition and associated hygroscopicity of the BC particles removed as well as their relative contribution to the atmospheric particle concentrations.

1. Introduction

[2]   Black Carbon (BC) is a ubiquitous and major component of aerosol particles generally related to combustion sources such as automobile exhaust, domestic exhausts, and biomass burning [*Andreae and Merlet*, 2001; *Bond et al.*, 2007; *Yan et al.*, 2011]. Recent studies in polluted urban environments show that as much as 80% of the submicron particle number size distribution contains some BC [*Moffet*

[1]Scripps Institution of Oceanography, University of California, San Diego, La Jolla, California, USA.
[2]Department of Civil and Environmental Engineering, Stanford University, Stanford, California, USA.

Corresponding Author: L. M. Russell, Scripps Institution of Oceanography, University of California, San Diego, La Jolla, CA 92093, USA. (lmrussel@ucsd.edu)

[3]Department of Chemistry and Biochemistry, University of California, San Diego, La Jolla, California, USA.
[4]School of Earth and Atmospheric Sciences and School of Chemistry and Biomolecular Engineering, Georgia Institute of Technology, Atlanta, Georgia, USA.
[5]Department of Civil and Environmental Engineering and Department of Engineering and Public Policy, Carnegie Mellon University, Pittsburgh, Pennsylvania, USA.
[6]Department of Civil and Environmental Engineering and Department of Chemical Engineering, California Institute of Technology, Pasadena, California, USA.

et al., 2008], which can contribute a large part of particle mass (as seen in some primary aerosols) or only a small core (as seen in some secondary particles). BC is strongly absorbing in both the visible and near-infrared spectrum, and its direct aerosol effect is estimated to be a principal contributor to global atmospheric warming [*Ramanathan and Carmichael*, 2008]. BC aerosol particles have an atmospheric lifetime of the order of one week [*Ogren and Charlson*, 1983; *Stier et al.*, 2007], orders of magnitude shorter than most greenhouse gases. Aerosol particles are not well mixed in the atmosphere but are instead geographically and temporally correlated to emission sources. Because their short atmospheric lifetime means immediate regional impacts on climate, reducing BC emissions has been proposed as a control strategy to offset short-term climate changes [*Jacobson*, 2002]. Aggressive control policies for diesel emissions in California have produced a near 50% decrease in BC concentrations (while non-absorbing particles have remained nearly constant), resulting in an estimated change in the direct radiative forcing of -1.4 W m^{-2} over the state [*Bahadur et al.*, 2011].

[3] In addition to warming the atmosphere through absorption of incoming shortwave radiation, BC particles also impact the climate in a series of feedbacks through their interaction with clouds and temperature [*Jacobson*, 2002; *Koch and Del Genio*, 2010]. BC particles internally mixed with or coated by hygroscopic species serve as efficient cloud condensation nuclei (CCN) for both warm and mixed-phase clouds [*Andreae and Rosenfeld*, 2008; *Dusek et al.*, 2006; *Koehler et al.*, 2009; *Lammel and Novakov*, 1995]. Perturbations to the BC concentration can therefore change the cloud droplet number (CDN) concentration and droplet size [*Roberts et al.*, 2003], which in turn influence both the cloud optical properties and cloud lifetime. Depending on the vertical distribution of aerosols, their mixing to the cloud deck, and meteorological conditions, these two so-called aerosol indirect effects tend to increase the cloud reflectance and cloud liquid-water path, respectively, and are thought to have a net cooling effect on the atmosphere [*Lohmann and Feichter*, 2005]. Competing semi-direct effects are found to decrease the cloud cover by stabilizing the atmosphere through warming [*Hansen et al.*, 1997] and to increase absorption by the cloud, helping to burn it off [*Jacobson*, 2006]. In contrast to the direct aerosol effect, the net climate forcing due to these cloud feedbacks and semi-direct effects is highly uncertain [*Forster et al.*, 2007] and may be either a significant offset, or addition, to the direct effect. An assessment of the degree to which the indirect effects of reducing BC offset or enhance the direct effects is needed to quantify the overall mitigation of climate change by BC on which policies can be constructed.

[4] General circulation models (GCMs) with explicit aerosol - cloud interactions are the principal tools for estimating global climatic impacts of aerosols. Recent GCM studies that have investigated the indirect effects of BC on CDN concentrations differ not only in magnitude, but also in the sign of the change in cloud droplet concentrations depending on the chemical properties of BC particles as well as the extent to which other indirect effects are explicitly modeled [*Bauer et al.*, 2010; *Chen et al.*, 2010b; *Koch et al.*, 2009; *Kristjansson et al.*, 2005; *Spracklen et al.*, 2011]. A recent multimodel comparison [*Koch et al.*, 2011]

investigating the effect of soot mitigation on liquid clouds concluded that soot removal could either increase or decrease the cloud droplet number with the final response depending on a combination of factors including the composition and size of the soot particles, the magnitude of soot change caused by emissions reduction, as well as the nonlinear response of the indirect effect itself. Although some generalized trends were found among the GCMs investigated, there was no consensus on the sign or magnitude of the cloud response in isolation to soot emission mitigation. In this work, we address this uncertainty by focusing on two models that account for different processes thus have produced different responses. *Chen et al.* [2010a] estimated that a 50% reduction in fossil fuel emissions would result in a 6% decrease in the globally averaged CDN concentration as a consequence of the first indirect effect; *Jacobson* [2010], who performed climate response simulations, reported a 1% increase in cloud droplet number concentration for complete removal (100% decrease) of fossil fuel soot emissions (but a 10% decrease when both fossil fuel and biomass burning emissions were removed). The increased drop concentration of *Jacobson* [2010] in the no fossil soot (NFS) simulation was the combined result of the modeled hydrophobicity of fossil fuel BC particles and the changes in cloud dynamics from semi-direct and cloud absorption effects of BC on temperature. The explicit treatment of feedbacks by *Jacobson* [2010] provides the more complete calculation of climate impacts between the two GCMs compared here. The scope of the present work focuses only on the change in CDN concentration from reducing BC particles. In this way we can evaluate one part of the climate benefit of a BC reduction.

[5] One source of uncertainty in calculating CDN changes is the simplifications of cloud droplet activation schemes that are used in GCM parameterizations to reduce computational time [*Meskhidze et al.*, 2005]. To assess this difference in modeling approaches, we employ a parcel model that connects detailed cloud chemistry and microphysics with a calculated supersaturation profile [*Guibert et al.*, 2003; *Snider et al.*, 2003]. Since the parcel model does not include the feedback of BC on the temperature profile, the semi-direct effects are not assessed in this study. Here, we use the *Russell and Seinfeld* [1998] parcel model.

[6] Another source of uncertainty in GCM predictions of BC indirect effects on CDN is the representation of aerosol composition, size, and concentration. To address this uncertainty, we assume internally and externally mixed BC particles, constrained by single particle measurements (using the Aerosol Time of Flight Mass Spectrometer, ATOFMS) at five California field sites in initializing the chemically detailed parcel model. California provides an ideal test case for this work due to the ready availability of high-resolution aerosol measurements that represent different emission conditions.

[7] The combined approach uses CDN concentrations calculated from chemically detailed size distributions initialized with measured aerosol concentrations. The impact of reducing BC is determined by repeating our model simulations for 50% reduction in BC compared with the base case, the results of which are also compared with GCM results from *Chen et al.* [2010a] and *Jacobson* [2010]. These comparisons allow us to address the following questions: (1) Does BC contribute significantly to cloud droplets in representative

Table 1. Summary of ATOFMS Field Campaigns Used in This Analysis

Location	Campaign	Dates	Coordinates (N, W)	Environment	References	IMPROVE Station	IMPROVE Station Coordinates (N, W)
Trinidad Head (TH)	CIFEX	Apr 2004	41.3, 124.9	Clean marine, long-range pollution	*Holecek et al.* [2005]	LAVO	40.5, 121.5
Riverside, (RV)	SOAR I	Aug 2005	33.5, 117.2	Highly polluted urban and regional transport	*Shields et al.* [2008]	SAGO	34.1, 116.9
La Jolla (LJ)		Dec 2006	32.5, 117.1	Polluted urban and biomass burning		JOSH	33.3, 116.3
Long Beach (LB)		Aug 2007	33.5, 118.9	Polluted marine and urban mix	*Ault et al.* [2009]	AGTI	33.4, 117.9
Sacramento (SA)	CARES	Jun 2010	38.3, 121.2	Polluted urban and long range transport		BLIS	38.9, 121.1

aerosol populations? (2) How do the aerosol and cloud number size distributions determined in GCMs compare with results from a detailed parcel model? (3) How does BC mitigation impact the total cloud droplet concentration?

2. Aerosol Case Studies

[8] To calculate the contribution of BC-containing particles to CDN concentrations, we initialized the parcel model with aerosol particle compositions measured in California. A number of ATOFMS field studies have been conducted to characterize external mixtures of aerosol particles in California, and here we use five studies to represent a range of chemical mixtures found in California aerosol populations. ATOFMS enables online size-resolved chemical characterization of ambient aerosol samples through information about the chemical fingerprints associated with each particle type [*Silva and Prather*, 1997; *Silva et al.*, 1999; *Suess and Prather*, 1999]. Specific details for the selected field studies used in this work are summarized in Table 1. The chemical characteristics of submicron carbonaceous aerosol particles have been established based on a comparative study [*Bahadur et al.*, 2010], and here we use a similar methodology to describe the aerosol observed at different field sites as an external mixture of four major particle types:

[9] 1. The Black Carbon (BC) type is characterized by a positive ion mass spectrum that is dominated by carbon atom clusters (C_n) with smaller signal contributions from organic carbon, nitrate, sulfate, and ammonium tracer fragments. The mass spectra are similar to spectra of particles sampled during source tests from vehicular exhaust [*Sodeman et al.*, 2005], suggesting that these particles are produced from primary sources of fossil fuel combustion and correspond most closely to atmospheric black carbon.

[10] 2. The Organic Carbon (OC) type is characterized by major OC peaks at +27 (C_2H_3) and +43 (C_2H_3O), a peak at +39 (K) associated with organics produced during biomass combustion, and positive ion fragments up to and beyond +150 indicative of high mass compounds that may be formed via atmospheric processing [*Silva et al.*, 1999].

[11] 3. Sulfate-type particles are characterized by a large peak at −97 (HSO_4) in the negative spectra.

[12] 4. Nitrate-type particles contain a large peak at −62 (NO_3) in the negative spectra. The nitrate and sulfate particles are often internally mixed; in these cases the

particle is classified as either sulfate or nitrate according to the larger peak.

[13] The sulfate and nitrate particle types typically do not produce positive ion spectra but are still likely to contain a carbonaceous core [*Pratt et al.*, 2010]. Even though all four of these particle types could contain BC nuclei and mass from combustion sources, we classify them here using their mass spectral signal as a signature for those particles that are most uniquely associated with fossil fuel emissions by vehicles. Spectra containing sea salt peaks are found in the coastal sites typically mixed with the sulfate and nitrate classes, and pure sea salt particles do not make up a significant fraction of the total detected submicron particles at these sites. Approximately 5–10% of particles do not fall into any of these categories and are classified as "other" and "not further chemically-resolved." The relative concentrations of each of these particle types can be determined by analyzing the ATOFMS measurements (using a nozzle inlet with a cutoff of 3 μm), but since the instrument detects larger particles with higher efficiency than smaller particles, unscaled number counts can be misleading [*Allen et al.*, 2000; *Bhave et al.*, 2002]. We assume that the relative fraction of each particle type within each size bin is statistically similar to the ambient particles allowing us to construct a relative size distribution (independent of absolute particle counts) for the different particle types., We use measurements from the co-located sizing instruments – Scanning Mobility Particle Sizer (SMPS, 0.01–1 μm), Optical Particle Counter (OPC, 0.5–2.5 μm), and Aerodynamic Particle Sizer (APS 1–25 μm) to determine the absolute aerosol number concentration between 0.01 and 2.5 μm, which in turn is multiplied by the ATOFMS particle fractions to reconstruct atmospheric number size distributions for each particle type. The size-dependent relative ATOFMS particle fraction and corresponding reconstructed number size distributions are illustrated in Figure 1 for the five sites.

[14] Characteristic densities for each of these particle types have been measured [*Qin et al.*, 2006] and are used to convert the number size distributions into mass size distributions. Finally, each particle type is treated as an internal mixture of five species – ammonium sulfate, ammonium nitrate, BC (represented as elemental carbon), OC (represented as a long chain carboxylic acid [*Russell et al.*, 2011]), and sea salt (represented as sodium chloride), allowing for the representation of carbonaceous cores in the sulfate and nitrate types and deposition of secondary species onto the BC and OC
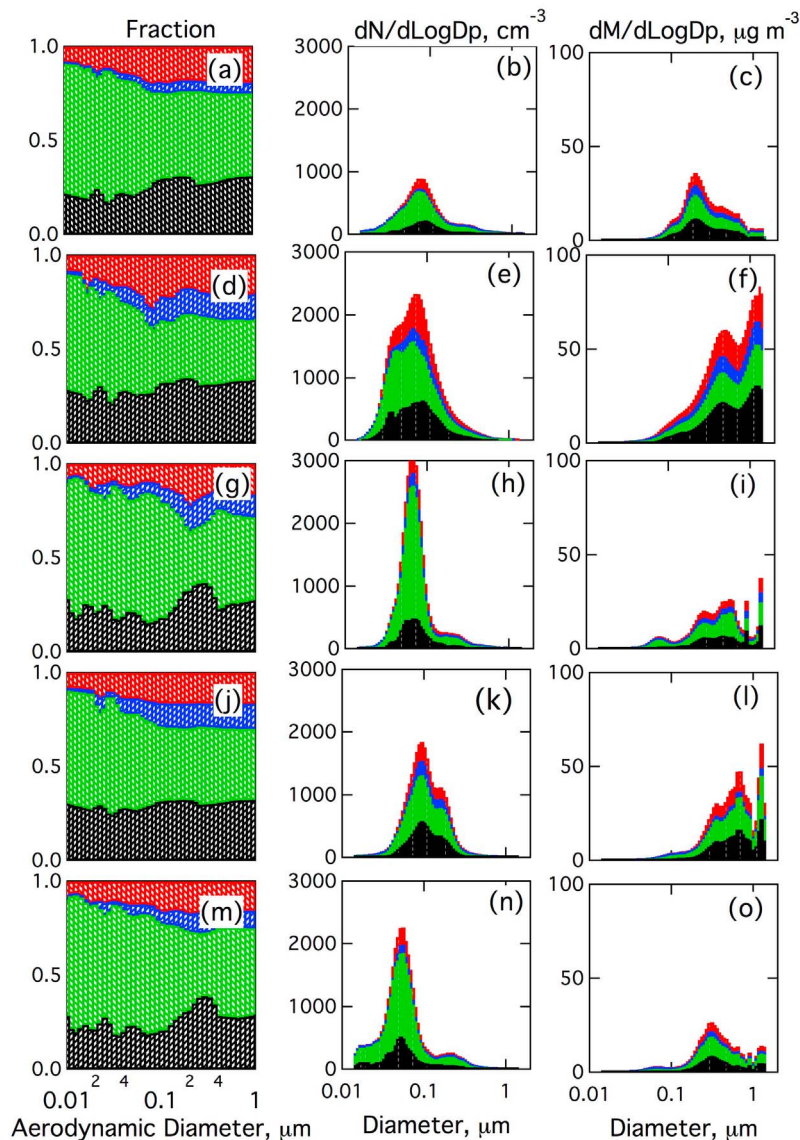
Figure 1. Size dependent population for the BC-type (black), OC-type (green), Sulfate-type (red), and Nitrate-type (blue) particle types described in section 2 at (a, b, and c) TH, (d, e, and f) RV, (g, h, and i) LJ, (j, k, and l) LB, and (m, n, and o) SA field sites. Figures 1a, 1d, 1g, 1j, and 1m illustrate the relative number fraction measured using the ATOFMS, Figures 1b, 1e, 1h, 1k, and 1n illustrate the number size distribution of each particle type (reconstructed from ATOFMS, SMPS, and APS measurements) in cm^{-3}, and Figures 1c, 1f, 1i, 1l, and 1o illustrate the corresponding mass distribution in $\mu g\ m^{-3}$.

types. We use a volumetric mixing rule with the densities of these pure species to constrain the relative mixing ratio to the observed density. Since multiple solutions are possible, the internal mixing state represents a possible composition rather than a unique one. Figure 2 illustrates the calculated composition of each of the four particle types that are used to represent the particle populations observed in the five case studies. The validity of these inferred mass-based internal mixing states for the four particle types can be examined by comparing the predicted total EC, OC, Sulfate, and Nitrate mass with measurements. We use filter-based measurements from nearly collocated monitoring sites operated as part of the IMPROVE network. Figure 3

shows the comparisons of PM2.5 mass monthly averages measured from the IMPROVE sites, combined ATOFMS and particle number measurements, and calculated values from the GCMs of *Chen et al.* [2010b] (who do not explicitly report nitrate mass) and *Jacobson* [2010]. We find relatively good agreement between the four mass measurements, with the GCMs also successfully reproducing the annual cycles in EC, OC, and Sulfate. Compared to the IMPROVE measurements, the single-particle-based measurements for the parcel model under-predict the EC and Nitrate mass by between 10 and 15% and over-predict the OC and Sulfate mass by between 5 and 15%. This discrepancy is reasonable considering the variability associated
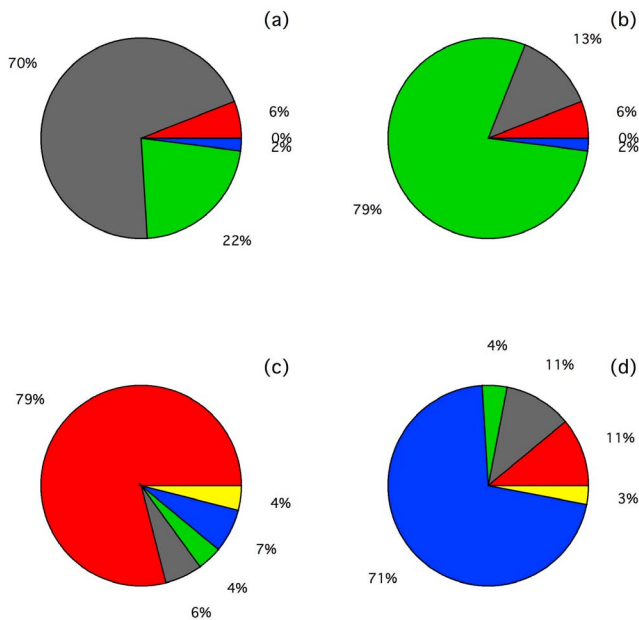
Figure 2. Calculated composition of each of the four types of particles used in the chemically detailed parcel model: (a) BC-type, (b) OC-type, (c) Sulfate-type, and (d) Nitrate-type externally mixed particles. Chemical species are Ammonium Sulfate (red), Ammonium Nitrate (blue), long chain carboxylic acids (green), EC (gray), and Sodium Chloride (yellow).

with using nearby measurements, monthly averaged values, and the uncertainties associated with the measurements.

[15] For the 50% BC reduction cases, we decrease the number concentration of the BC-type particles by half while preserving the shape of the size distribution – the underlying assumption being that a reduction in BC emissions reduces the number concentration of BC-type particles by half but does not alter the mean size. The size distributions and mass of the other particle types are preserved as measured (including the small BC mass component). The overall effect on the aerosol is a loss in mass between 0.16 $\mu g\ m^{-3}$ (TH) and 0.50 $\mu g\ m^{-3}$ (RV), which corresponds to a reduction of between 5% and 7% in particle mass or between 7% and 11% in particle number concentration. Since BC is co-emitted with many other particle components, it is likely that an actual reduction of BC emissions would also reduce the OC, nitrate, and sulfate particle types that constitute the other particle types. In fact, all three of these particle types may have BC cores, but, as a first approximation, we remove half of only the BC particle types.

3. Microphysics Modeling Approach

[16] The aerosol dynamics model [*Russell and Seinfeld*, 1998] used in this study is based on a fixed-sectional approach that represents the detailed chemical composition of particles as both internally mixed components and externally mixed particle types (or populations). Each particle type is described by size-dependent internal mixtures of five chemical components: Ammonium Sulfate, Ammonium Nitrate, long chain carboxylic acids, Elemental Carbon (EC), and Sodium Chloride. The model tracks the aerosol

microphysics accounting for particle growth, coagulation, evaporation, condensation, nucleation, and cloud droplet activation mechanisms. The gas phase and heterogeneous sulfur chemistry are also described explicitly but are negligible in the short simulations conducted here. Water is treated in a moving section representation allowing for the accurate calculation of evaporation and condensation depending on the relative humidity, and both the particle mass and particle number concentration are tracked using a dual moment method. The maximum supersaturation, CDN concentration, and equivalent cloud droplet radius are calculated kinetically based on the detailed chemical composition of each particle type and size rather than from equilibrium Köhler theory, providing a more flexible treatment of warm stratus clouds where the time scale for change of supersaturation can be comparable to or smaller than the time scale for particle growth. The parcel model captures the dynamical variability in the supersaturation and applies It to the particle size distribution, while GCMs apply a single average velocity or a probability distribution of velocities (prescribed or diagnosed from large scale dynamics) to describe changes in cloud droplet number [*Morales and Nenes*, 2010].

[17] To provide a simple yet relevant cloud thermodynamic structure that can be used for all five cases, we use a continentally influenced marine stratus cloud as a model cloud. Profiles of meteorological variables that were collected on a flight of the Monterey Area Ship Track (MAST) experiment on JDT 178 [*Durkee et al.*, 2000] in a continentally influenced cloud layer from 173 to 405 m above sea level are used to describe the temperature profile, humidity profile, and total amount of available liquid water. The total available water vapor in the cloud is 0.35 g m^{-3} and the cloud base temperature is 285.3 K. The frequent presence of low lying stratocumulus clouds off the coast of California, particularly in the spring and summer months [*Lu et al.*, 2007], suggests that this is a reasonable and relevant set of meteorological conditions for offshore flow, despite being a simplification over GCMs that include all cloud regimes, including mixed-phase clouds.

[18] The parcel updraft velocity was calculated in two modes: (1) the fixed updraft mode with a constant updraft velocity for an observed range of values of 0.2 and 2.0 m s^{-1} [*Nicholls and Leighton*, 1986] is used to establish representative values for maximum supersaturation, cloud droplet number concentration, and typical duration of a single cloud cycle, as in *Russell et al.* [1999]; and (2) the calculated updraft mode initialized by a surface temperature difference of +1.0 K relative to the ambient at sea level [*Lucas et al.*, 1994]. The calculated updraft mode follows the treatment of *Pruppacher and Klett* [2003] developed for convective clouds, calculating the updraft velocity at each time step while allowing the adiabatic cooling of the aerosol parcel and entrainment of humid air. The changes in temperature and updraft velocity that are evaluated simultaneously are

$$dT = -\left(\frac{gUdt + L\Delta w + \varphi\left[L\Delta w + c_p(T - T_a)\right]}{c_p} \right) \quad (1)$$

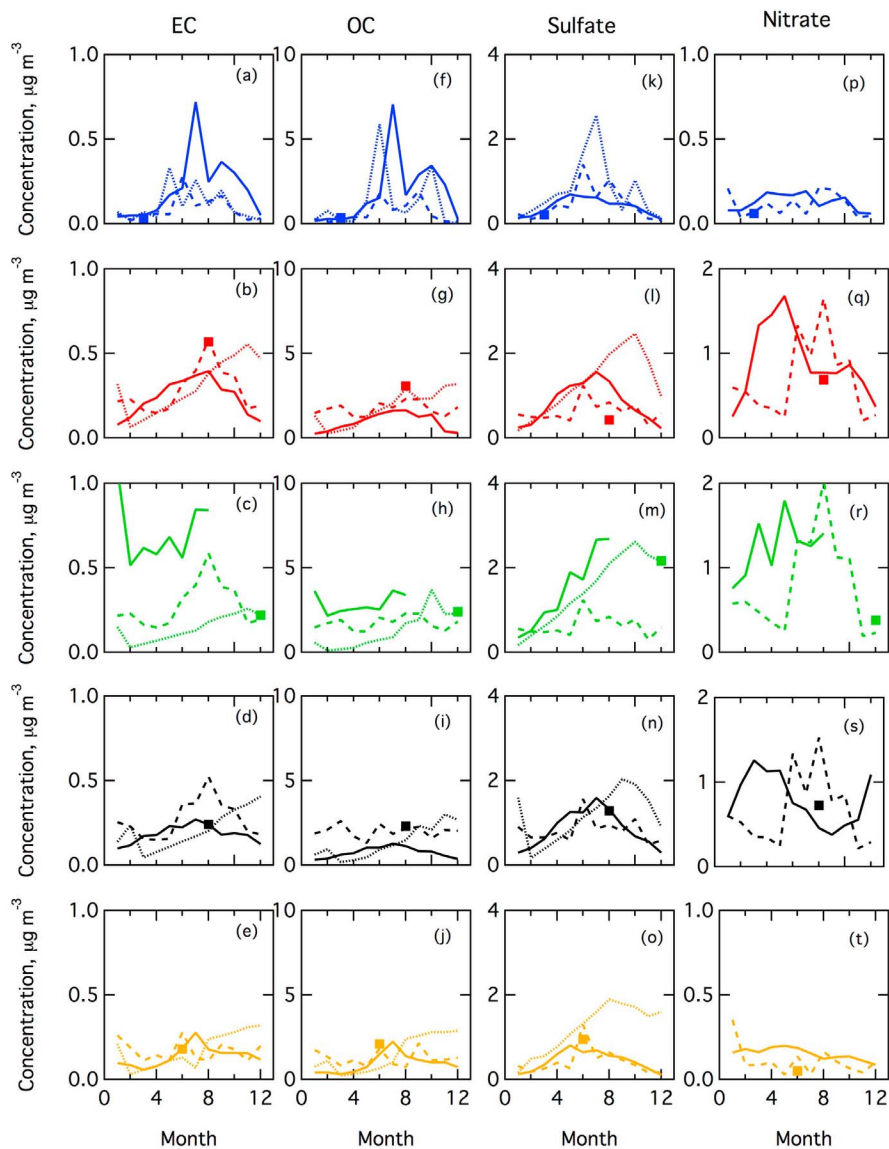$$dU = \left[\frac{2g}{3}\left(\frac{T - T_a}{T_a} - w \right) - \frac{2\varphi}{3}U^2 \right]dt \quad (2)$$

Figure 3. Monthly averages for the total PM2.5 mass concentration of (a–e) EC, (f–j) OC, (k–o) Sulfate, and (p–t) Nitrate at the TH (blue), RV (red), LJ (green), LB (black), and SA (orange) sites. Solid lines are filter based measurements from nearly collocated IMPROVE network sites at LAVO (blue), SAGO (red), JOSH (green), AGTI (black) and BLIS (orange). Dashed lines are from *Jacobson* [2010] and dotted lines are from *Chen et al.* [2010b]. Squares show monthly averages based on ATOFMS and particle size measurements used for initializing the parcel model. IMPROVE data is illustrated for 2006, with bars showing the 10 year variability from 2001 to 2010.

where T is the parcel temperature, T_a is the ambient temperature, g is the acceleration due to gravity, w is the liquid water mixing ratio, L is the latent heat of condensation of water, c_p is the specific heat of water, ϕ is a dimensionless entrainment parameter computed based on the liquid water profile determined using a fixed updraft velocity, t is time, and U is the updraft velocity.

[19] Figure 4 illustrates the simulated parcel altitude, relative humidity, liquid water content, and updraft velocity for the five case studies using both the measured aerosol concentrations and similar cases but with BC reduced by 50% BC. The simulation is initialized with the aerosol parcel at rest (U = 0) at sea level with a potential temperature that is 1 K in excess of the measured surface temperature in the sounding of the atmosphere. This 1 K excess means that, in the first stage of the simulation, the parcel is warmer than the surrounding air and accelerates upwards. As the air parcel ascends it is cooled by expansion, reaching a temperature first equal to, and then less than the surrounding air. Therefore it attains a maximum updraft velocity (U = 1.4 m s^{-1} for the conditions simulated here) before starting to decelerate. In the second stage of the simulation (starting at approximately 150 s), the parcel enters the supersaturated region and the available water vapor starts to condense onto the cloud
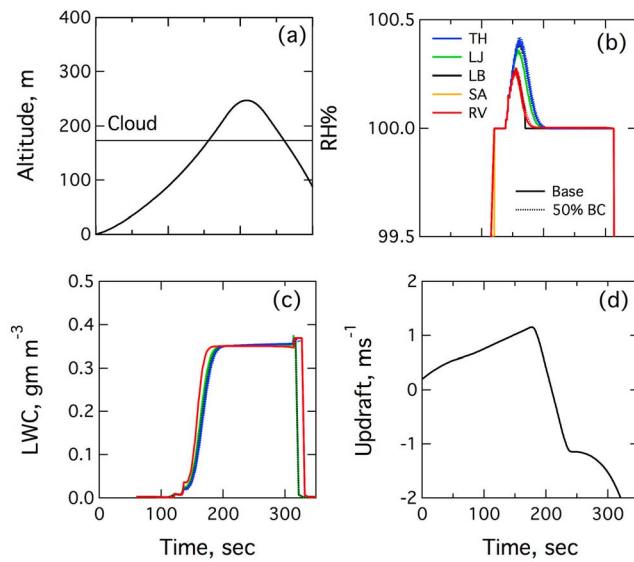
Figure 4. Parcel model simulations of the (a) Altitude, (b) RH, (c) liquid water content, and (d) updraft velocity for TH (blue), RV (red), LJ (green), LB (black), and SA (orange) over a single cloud cycle. Solid lines show the base case and dashed lines show the 50% BC case.

condensation nuclei (CCN). The supersaturation reaches a maximum value (between 0.24% at RV and 0.38% at TH) and then starts to drop as the water vapor condenses. In the third stage of the simulation (starting at approximately 220 s), the aerosol has a negative velocity and starts to descend, eventually leaving the cloud. In the final stage of the simulation (starting at approximately 310 s), the aerosol parcel descends through the unsaturated layer below the cloud, and rapidly loses all condensed water. For the cloud used in this study, a single cloud cycle typically lasts 300 s after which the simulation is terminated, i.e., the downdraft leg outside the cloud is neglected. This time is sufficient for the parcel to achieve the maximum supersaturation, to condense the available liquid water, and to start to descend in the subsequent downdraft. The 50% BC cases result in a higher maximum supersaturation relative to the base case (for example, 0.42% compared to 0.40% at TH, and 0.25% compared to 0.24% at RV) and the condensation of liquid water is slightly slower. The updraft velocity profiles are identical in all cases, indicating that the small differences in the rate of water condensation in the different cases do not have an appreciable effect on the updraft velocity, since the difference in amount of latent heat released is relatively small.

[20] Figure 5 illustrates the evolution of the BC particle size distribution at the start of the simulation, in-cloud, before maximum supersaturation, and in-cloud, after maximum supersaturation. In addition to the change in modal diameter as a result of growth of all particles due to cloud processing, a secondary mode at approximately 10 μm and larger is seen, which we define to be the activated mode [Cantrell et al., 1999; Erlick et al., 2001] that can be integrated to determine the total number of cloud droplets formed and mean cloud droplet diameter. The cut-off diameter for this mode is

identified from the number size distribution for each particle population following activation.

[21] The impact of varying the updraft velocity in the constant updraft mode (and variations in the prescribed surface temperature difference and entrainment in the calculated updraft mode) on the maximum supersaturation and CDN concentration is illustrated in Figure 6. For the calculated updraft, both the updraft velocity at the point of maximum supersaturation and the mean updraft velocity up to that point are shown. Prescribing a surface temperature difference between 0.5 and 1.5 K produces mean updraft velocities between 0.3 and 0.9 m s^{-1} that are consistent with field measurements in clouds [Emanuel and Bister, 1996; Nicholls and Leighton, 1986]. Faster updrafts allow for a higher maximum supersaturation (0.3% and 0.5% respectively), and the trend is consistent with the constant updraft mode, where fixed updraft velocities between 0.2 and 1.6 m s^{-1} produce maximum supersaturation varying between 0.3 and 1.0%. The CDN concentration varies by a small amount between 312 cm^{-3} and 283 cm^{-3} over this range of velocities, indicating that activation determined kinetically by integrating the largest size mode is limited by
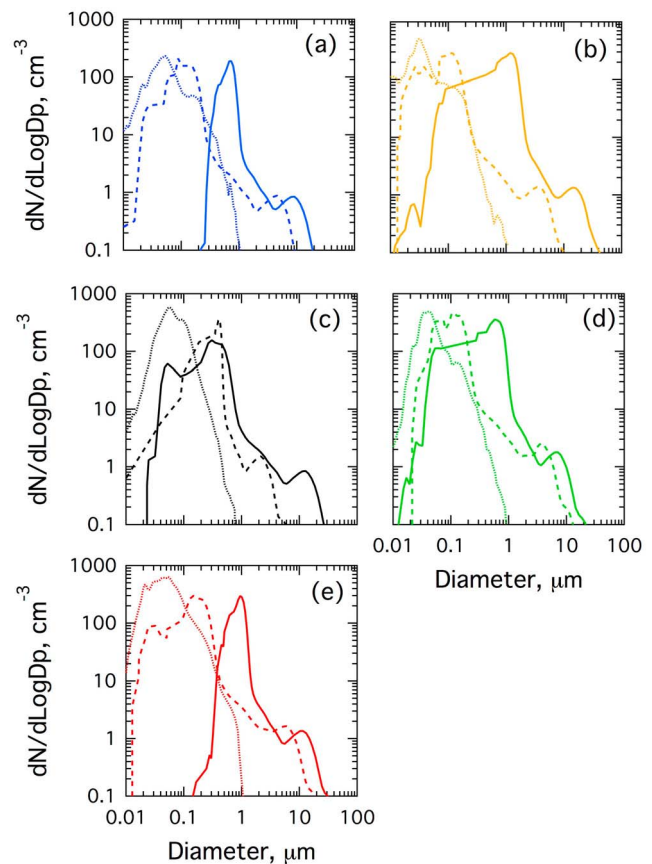

Figure 5. Parcel model simulations of the BC particle size distribution from (a) TH, (b) SA, (c) LB, (d) LJ, and (e) RV cases. Dotted lines are below cloud (t = 50 s), dashed lines are in-cloud before max RH (t = 150 s), and solid lines are in-cloud after max RH (t = 250 s). Particles in the secondary mode around 10 μm are considered activated.
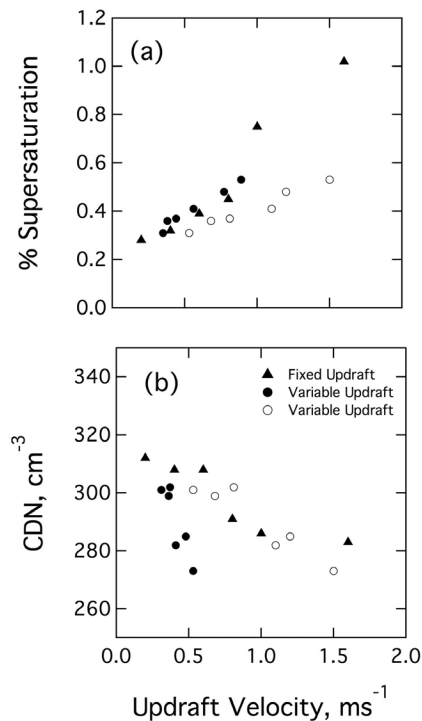
Figure 6. Parcel model simulations of the dependence on the updraft velocity operating in fixed updraft (triangles) and energy conservation (circles) mode: (a) maximum supersaturation and (b) cloud droplet number concentration. Empty circles indicate updraft at maximum supersaturation and filled circles indicate mean updraft velocity up to the maximum supersaturation.

the total amount of available water vapor and aerosol concentration rather than updraft conditions.

4. Case Studies

[22] The number concentration of aerosol particles, the number concentration of activated cloud droplets, the maximum supersaturation, and the mean cloud droplet diameter

are summarized in Table 2 for the base case and the 50% BC reduction case for each of our case studies. We find that several consistent trends are observed across sites for both the base case and the 50% BC reduction case. First, the number concentration of cloud droplets (between 160 cm^{-3} at TH and 301 cm^{-3} at RV) is directly correlated to the number concentration of aerosol particles (7287 cm^{-3} at TH and 14321 cm^{-3} at RV), while the average droplet diameter is inversely related. This indicates that a large number of potential CCN compete with each other under these polluted conditions. The total liquid water in the parcel in each simulation reaches the maximum available water from the cloud. Second, a higher maximum supersaturation (0.38% at TH) is attained with a corresponding higher updraft velocity (0.92 m s^{-1} at TH) at lower aerosol concentrations indicating that the maximum supersaturation is limited by the size of the CCN sink, and the faster condensation in the more polluted cases releases latent heat more quickly, balancing the available buoyant force and resulting in slower updraft velocities.

[23] A more interesting trend is observed when comparing the reduction in cloud droplet number concentrations in the 50% BC case to the base case. Since the BC particle type typically comprises between 20% and 30% by number of the total particles, the 50% BC reduction causes between 7% (at TH) and 11% (at LB) reduction in the particle number concentration. The decrease in particle number concentration of cloud drops however is only between 5% (at TH and RV) and 9% (at LB). This implies that in addition to the total size distribution, the differences in aerosol chemical composition between the TH and LB cases are also a contributing factor to the differences in activation of cloud droplets. The particle number concentration and fraction of particles activated for each case study are illustrated in Figure 7 resolved by the four externally mixed particle types. The OC particles comprise the largest fraction of the total droplets (between 42% at RV and 55% at TH) and the nitrate particles comprise the smallest fraction (between 8% at TH and 16% at LB) consistent with the relative abundance of these particle types. Activated BC particles make up between 16% (at LB) and 20% (at TH) of the total cloud droplets. A much larger fraction (between 4% and 8%) of the more hygroscopic

Table 2. The Number Concentration of the Total Aerosol Particles (N$_a$), Black Carbon Particles (N$_b$), Cloud Droplets (N$_c$), Black Carbon Cloud Droplets (N$_{bc}$), Total and Percent Difference in Aerosol Mass (Δm), Average Cloud Droplet Diameter (D$_c$), Maximum Supersaturation (S$_{max}$), and Corresponding Updraft Velocity (U)[a]

Location	N$_a$ (cm^{-3})	N$_b$ (cm^{-3})	N$_c$ (cm^{-3})	N$_{bc}$ (cm^{-3})	$-\Delta$m (μg m^{-3}) (Percent)	S$_{max}$ (%)	D$_c$ (μm)	U (at S$_{max}$) (m s^{-1})	S$_{par}$ (%)	N$_{par}$ (cm^{-3})
					Base Case					
TH	7287	1015	160	31		0.38	9.8	0.92	0.43	202
RV	14321	2130	301	59		0.24	8.6	0.83	0.27	338
LJ	10178	2112	216	64		0.27	9.3	0.86	0.31	243
LB	11295	2656	239	111		0.25	8.7	0.86	0.27	268
SA	9231	1686	191	77		0.34	9.0	0.87	0.37	227
					50% BC Case					
TH	6780	508	151	17	0.16 (6%)	0.40	10.2	0.92	0.46	192
RV	13286	1065	284	28	0.50 (7%)	0.25	9.8	0.83	0.29	323
LJ	9122	1056	202	31	0.28 (5%)	0.34	9.6	0.86	0.39	219
LB	9987	1328	216	55	0.31 (6%)	0.30	8.7	0.86	0.32	223
SA	8388	843	178	38	0.25 (7%)	0.38	9.1	8.87	0.40	187

[a]The maximum supersaturation (S$_{par}$) and droplet concentration (N$_{par}$) calculated using the *Nenes and Seinfeld* [2003] parameterization are also listed.
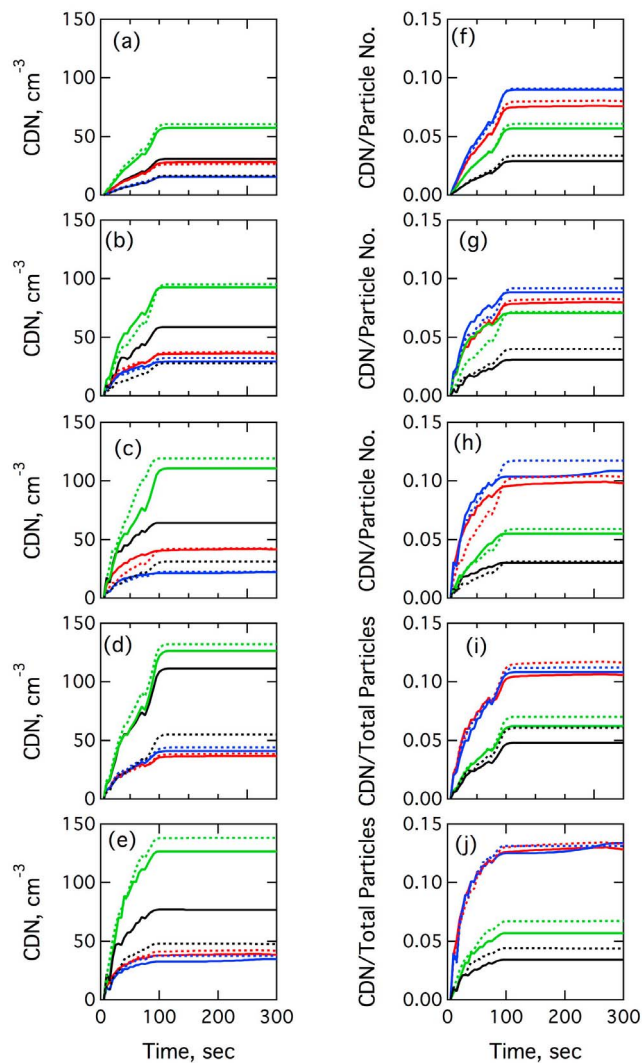
Figure 7. Parcel model simulations of the (a–e) cloud droplet number concentration and (f–j) fraction of particles activated for externally mixed particle populations corresponding to BC-type (black), OC-type (green), Sulfate-type (red), and Nitrate-type (blue) particles for a single cloud processing cycle. The base (solid lines) and 50% BC (dashed lines) cases are illustrated for TH (Figures 7a and 7f), RV (Figures 7b and 7g), LJ (Figures 7c and 7h), LB (Figures 7d and 7i), and SA (Figures 7e and 7j).

nitrate and sulfate particles activate compared to the less hygroscopic OC and BC particles (between 1% and 3%). In the 50% BC case, the total number concentration of activated BC droplets decreases, however this decrease is balanced to a certain extent by an increase in the number concentration of activated particles from the other three species. The climate implication of this result is that if only BC particles are reduced (in polluted environments), the many CCN that do not contain BC still activate in place of the BC aerosol particles preserving the cloud droplet populations and mean diameters. Even though the decrease in CDN is much less than proportional to the BC reduction (due to an associated increase in the number of activated

non-BC particles), the net effect of BC reduction is a small decrease in the total CDN concentration.

5. Comparison With GCM Simulations

[24] The total number concentration, composition, and mean size of the cloud droplets determine the cloud optical properties that, in turn, contribute to the quantitative radiative impact on the climate. Since the primary goal of this study is to understand the impact of BC mitigation on the aerosol indirect effect we can compare the CDN concentrations determined in this study with those from two state-of-the-art GCM simulations to evaluate the magnitude and trend in the change in cloud droplet concentration. In this work, we compare with the global model runs of GISS-TOMAS (a combination of Goddard Institute for Space Studies and Two Moment Aerosol Sectional models) [*Adams and Seinfeld*, 2002; *Chen et al.*, 2010b] and GATOR-GCMOM (Gas, Aerosol, Transport, Radiation, General Circulation Meso-scale and Ocean Model) [*Jacobson*, 2010] models. We chose these models for comparison because they had completed BC-reduction experiments. In brief, the *Chen et al.* [2010b] model tracks the size-resolved mass and number aerosol concentrations that are used to calculate cloud droplet concentrations using the parameterization of *Nenes and Seinfeld* [2003] with the kinetic modification introduced by *Fountoukis and Nenes* [2005], and a geographical resolution of 4° latitude × 5° longitude. For evaluating the aerosol indirect effect, changes to the cloud albedo and lifetime are calculated. *Jacobson* [2010] used a global-to-regional scale nested model in which two domains were explicitly treated: a global and a California domain. The California domain was resolved at 0.15 degrees (~13 km) west-east × 0.2 degrees (~22.2 km) south-north. Cloud microphysics (liquid, ice, and graupel) were solved explicitly with size and composition resolution, while cloud thermodynamics were considered to be at quasi-equilibrium. In making this comparison between GCM results and these five detailed case studies, we note the following differences that will necessarily make the comparison indirect: (1) GCM aerosol concentrations are constrained by emission inventories, while the parcel model is initialized by monthlong intensive observations of ambient concentrations, (2) GCM values represent a grid-cell average around the sampling site as opposed to a point measurement, and (3) GCM cloud droplets are based on predictive meteorological fields whereas the detailed chemical model uses a single thermodynamic profile of a polluted stratocumulus cloud. For all of these reasons, we expect some variability between the parcel model and the GCM calculations of CDN.

[25] Figures 8a–8c compare the total aerosol size distributions at the five California sites. The GCM-simulated size distributions agree well with the measured size distributions in the 0.05 to 1 μm size range but are higher by a factor of approximately 5 in the ultrafine size range (below 0.1 μm diameter). Since the number size distribution can be dominated by a large number of very small particles in a polluted environment, this difference can be explained by the difference in the smallest size bins used across the models; these smallest particles however are unlikely to impact significantly the total aerosol mass and rarely activate to cloud droplets. The difference in size distributions between this work and the *Jacobson* [2010] model is more
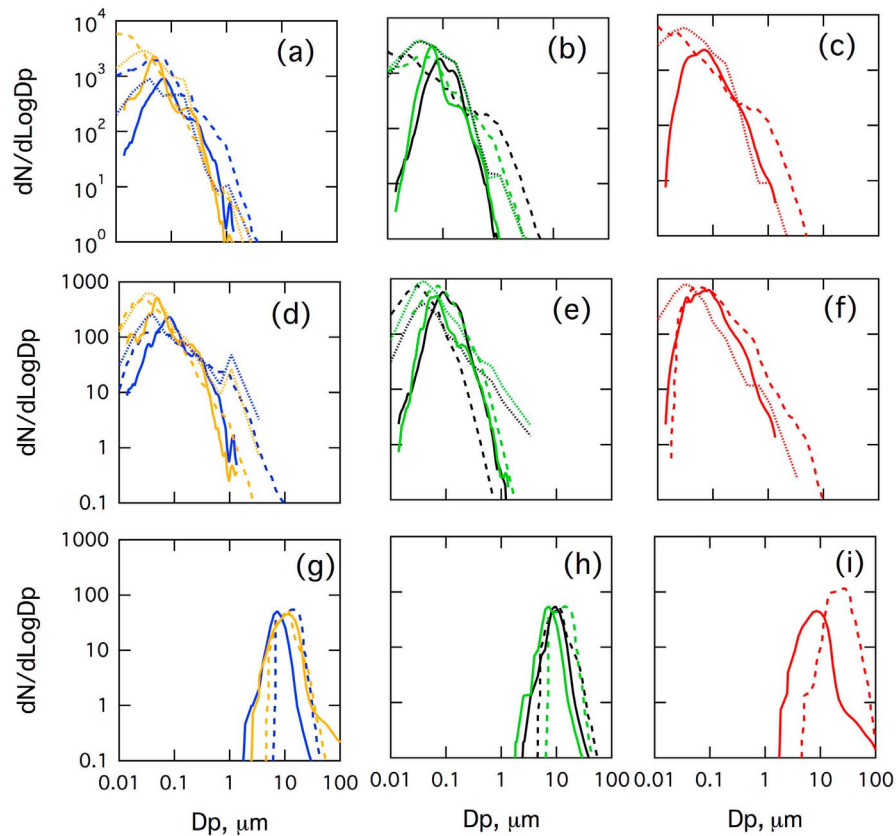
Figure 8. Comparison of the number size distribution of the (a, b, and c) total particles, (d, e, and f) BC type particles, and (g, h, and i) Cloud droplets. Line colors indicate the sites: TH (blue), SA (orange), LB (black), LJ (green), and RV (red). Solid lines show results from the parcel model, dashed lines are from *Jacobson* [2010], and dotted lines are from *Chen et al.* [2010b].

pronounced at larger sizes relative to the *Chen et al.* [2010b] model, particularly the supermicron size range. This difference is likely due to the omission of large mineral dust in the parcel model. The absolute number of these particles, however, is small compared with the submicron particles so that they do not significantly impact CDN concentrations.

[26] The total and BC-type particle number size distributions are illustrated in Figures 8d–8f. Here the difference is more pronounced, with the BC particles in the *Jacobson* [2010] model being slightly larger compared to the other two distributions. This difference arises primarily from the differences in the simulation of BC particles from biomass burning. Both *Chen et al.* [2010a] and *Jacobson* [2010] find a larger decrease in the BC burden when the biomass burning emissions are reduced in addition to fossil fuel emissions consistent with BC in biomass burning processes. In this work, we classify particles dominated by secondary and biomass tracers in the OC category. Thus the BC particles are more representative of fresh fossil fuel emissions and are smaller compared with the GCMs. Finally, Figures 8g–8i compare the size distribution of the total activated droplets (which are not computed in the *Chen et al.* [2010b] model that tracks the total water content and droplet number only). We find that both the modal diameter and total number concentration of cloud droplets agree well given the variety of differing assumptions in the three models, with

particularly good agreement at the pristine TH location. The larger number concentration of droplets from the GCM can be attributed to the higher particle number concentrations discussed above.

[27] Figure 9 compares the number concentrations of particles and cloud droplets from the GCMs and the parcel model. For the purposes of constraining the BC mitigation effect, the half-fossil fuel BC case is used from *Chen et al.* [2010b] and the no fossil soot (NFS) case is used from *Jacobson* [2010] (but the latter is only available from the global run as a Northern Hemisphere average). The primary trend that is observed is the direct correlation in the number concentrations for both total aerosol particles and total CDN concentrations of the three models, i.e., all three models predict a higher concentration in the more polluted cases. Relative to this study, both GCMs have a larger absolute concentration by between 20 and 25% as discussed in the previous section. Both GCMs also predict a larger total concentration for the CDN concentrations, by between 17% and 22%. This comparison represents quite good agreement for the base case given that the GCMs predict aerosol concentrations from emission inventories, transport, and removal processes whereas the parcel model used five sets of short-term observations.

[28] Slightly larger differences are observed in the relative changes between the base cases and the BC mitigation cases
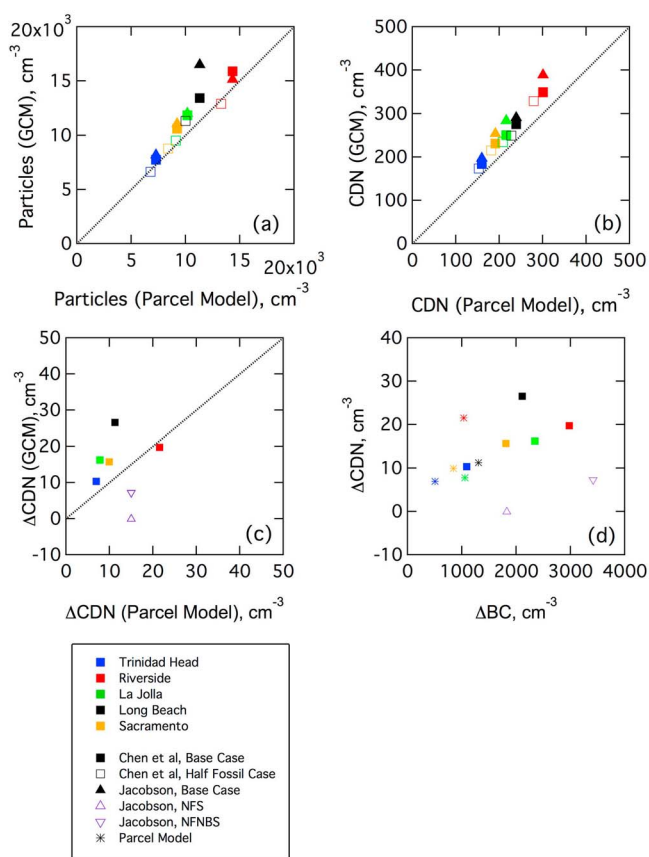
Figure 9. Comparison of (a) total particles, (b) activated cloud droplet number, (c) change in the droplet concentration (defined as base case-BC mitigation case), and (d) dependence of change in droplet number on change in BC-type particle number from this study at TH (blue), SA (orange), LB (black), LJ (green), and RV (red) with the GISS [*Chen et al.*, 2010b] (squares) and GATOR-GCMOM [*Jacobson*, 2010] (triangles) GCMs. Empty squares represent the half-fossil case from *Chen et al.* [2010b] and empty triangles show the range of the no fossil soot and no fossil/biomass soot values averaged for the Northern Hemisphere.

among the GCMs and the parcel model. Compared with the 7% to 11% decrease in particle number concentration from the parcel model, *Chen et al.* [2010b] find a larger decrease of between 18% and 20%. This larger reduction in particle number concentration by the *Chen et al.* [2010b] model is the result of their estimated decrease in the number concentrations of sulfate and organic particles from secondary particle formation associated with the reduced BC emissions (which are not identified by the ATOFMS characterization used in this study). *Jacobson* [2010] removed all fossil soot emissions and found a decrease slightly smaller than the observationally constrained particle concentrations in the parcel model of between 3% and 8%.

[29] The change in CDN concentration for the reduced-BC cases largely tracked the reductions in BC aerosol concentration, with the *Chen et al.* [2010b] model finding the largest reduction, the *Jacobson* [2010] model finding the smallest magnitude change, and the chemically detailed,

observationally constrained parcel model in between. The parcel model found that the 50% BC case decreased CDN concentrations between 6% and 9%, which is comparable to the 9% to 12% decrease found by *Chen et al.* [2010b]. The larger decrease of *Chen et al.* [2010b] tracks the larger decrease in BC particle number concentration, as shown in Figure 9. On the other hand, *Jacobson* [2010], whose model included climate feedback and semi-direct effects, reported an increase in CDN concentration of 1% when fossil fuel emissions were eliminated. This increase was consistent for both the northern hemisphere and the global average in that study, but was not calculated for the nested-domain California studies discussed here.

[30] BC particles in the *Chen et al.* [2010b] GCM and the parcel model are internally mixed with soluble species (such as organic acids, Ammonium Sulfate, and Ammonium Nitrate), making them somewhat hygroscopic. The *Jacobson* [2010] GCM treated fossil-fuel soot as evolving from externally mixed to internally mixed. It was emitted into its own size distribution and could internally mix by coagulating into a separate size distribution containing other chemicals or by condensation of gases onto its own distribution. As a result, it was initially mostly hydrophobic but became more hygroscopic with aging. Biofuel soot, on the other hand, was more hygroscopic upon emissions because it was coated with more soluble chemicals and organic carbon. The no-fossil-soot case of that model then corresponds to the removal of particles that were not so effective in acting as CDN, producing no significant corresponding reduction in the CDN concentration for the northern hemisphere or the global average. A better comparison for California BC particles may be to the case that removes both fossil soot and biofuel burning soot, since the biofuel burning BC particles were modeled as more hygroscopic (which is consistent with the BC measured in California) and because the larger overall BC reduction represents a larger fraction of the average concentration (which is more similar to reducing only fossil fuel BC in California, since fossil fuel BC is a large fraction of the atmospheric concentration). Other reasons that the *Jacobson* [2010] model has a smaller change in CDN in the no-fossil-soot only case are that it included the semi-direct effect [*Hansen et al.*, 1997] and the cloud absorption effect [*Jacobson*, 2006] and precipitation changes, all of which can affect cloud droplet concentration. These climate feedback effects are not included in the *Chen et al.* [2010b] GCM or the parcel model calculations.

6. Resolving Model Differences

[31] Although the parcel model and GCMs described in this work show some agreement in the total aerosol and CDN concentrations for California, the models have significantly different treatments, including of the aerosol microphysical state, cloud processes, activation mechanisms, and climate feedbacks. Further, they test a different set of mitigation scenarios – with the GCMs using an emissions-up approach and the parcel model relying on modifying measured aerosols. In this section we attempt to isolate and resolve some of these differences by performing additional calculations that extend the case studies described in Sections 3 and 4.
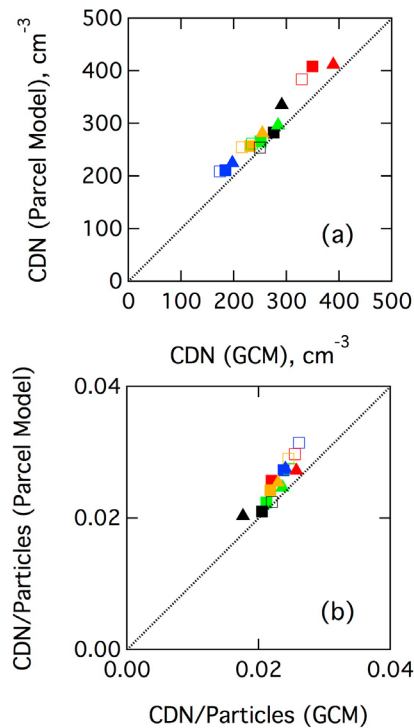
Figure 10. Comparison of the (a) total CDN and (b) CDN/Particle ratio determined from the GCMs using a full climate simulation, and by applying the parcel model and meteorology described in this work to the aerosol concentrations determined from the GCMs. The symbols used are the same as Figure 9.

[32] Figure 10a compares the CDN determined by applying the parcel model in conjunction with the marine stratocumulus cloud described in this work with the available GCM aerosol size distributions of *Chen et al.* [2010b] for both the base case and BC mitigation case, and *Jacobson* [2010] for the base case (since detailed aerosol information for the mitigation case in California is not available). The different aerosol species (sulfate, EC, OC, and nitrate) are treated here as externally mixed. This comparison preserves the aerosol microphysical properties and therefore isolates the combined effect of the activation mechanisms and meteorology between the parcel model and the GCMs. In general, applying the parcel model produces CDNs that are between 2% (LB) and 16% (RV) higher than calculated by the GCMs for the base cases. For the corresponding BC reduction cases, the corresponding increase is between 2% (LB) and 11% (RV), indicating that the enhancement is higher for cases with a larger fraction of hygroscopic (non-BC) particles. Figure 10b compares the fraction of total particles activated into cloud droplets for the corresponding cases. The trend is reproduced consistently, and a higher fraction of particles is seen to activate when the relative fraction of BC type particles is reduced.

[33] The effect of the internal mixing states for the aerosol population types described in Section 2 is examined by comparing the total number of CDNs determined by allowing internal mixing as described, and by treating each species as being only externally mixed – i.e., the nitrate type cies as being only externally mixed – i.e., the nitrate type particles are only nitrate and the BC type particles are only BC. The number size distributions for each particle type are unchanged, conserving the total number of aerosol particles. This experiment preserves the aerosol size and number, meteorology, and activation mechanisms, and isolates the effect of chemical composition. The change in CDN concentrations is illustrated in Figure 11 for ten simulation cases. The number of activated sulfate and nitrate particles are found to increase in each case, but typically by less than 5%. This is consistent with the bulk of these particles with internal mixing being composed of highly hygroscopic species that dominate the solution equilibrium. For the OC particle types, the number of activated particles is found to decrease by between 5% and 8%. This decrease is consistent with the reduction in hygroscopicity for this particle type when the sulfate and nitrate mass is replaced by OC. The biggest change is seen for the BC particle type, where the number of activating particles is reduced by between 70% and 80% compared to the case with internal mixing. Due to the relatively high supersaturation, some of the hydrophobic BC particles still activate, but this number is small compared to when some internal mixing with hygroscopic species is allowed. These trends support the result that the CDN change is more sensitive to change in BC concentration when the BC is at least partially hygroscopic.

[34] A recent study [*Ghan*, 2011] compared a number of complex cloud activation parameterizations and found significant differences in the maximum supersaturation and critical droplet diameters depending on the aerosol properties and updraft conditions. To isolate specifically the differences in activation between the parameterizations used in GCM studies and the explicit kinetic activation calculated by the parcel model, we have applied the parameterization of *Nenes and Seinfeld* [2003] to the measured aerosol size distributions in this work. The temperature, pressure, and
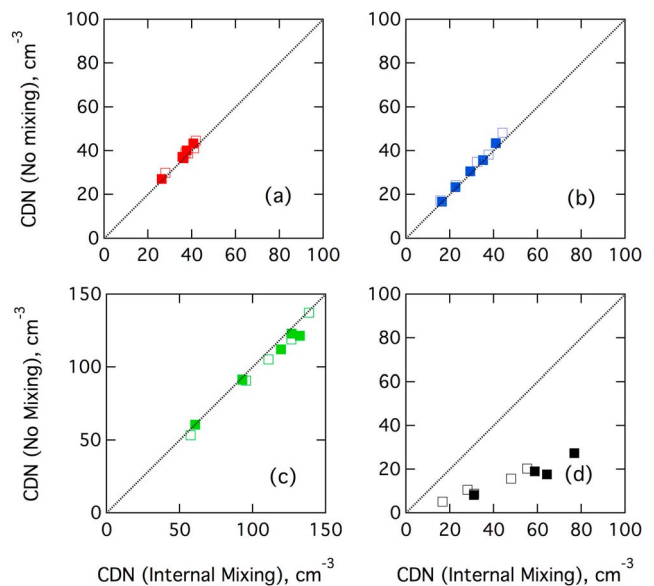

Figure 11. The total number of particles activated for (a) Sulfate, (b) Nitrate, (c) OC, and (d) EC type particles when no internal mixing is allowed, compared to the internal mixing states illustrated in Figure 2.
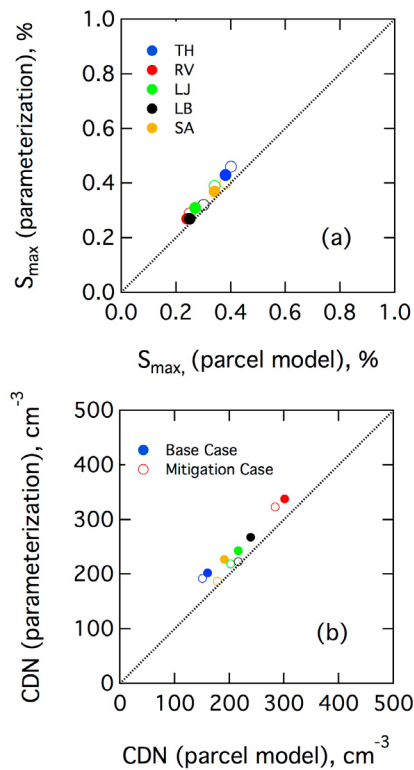
Figure 12. Comparison of the (a) maximum supersaturation and (b) cloud droplet number determined using measured aerosol size distributions by application of the *Nenes and Seinfeld* [2003] parameterization and the parcel model for the cloud conditions described in this study.

updraft conditions at the cloud base are used to determine the maximum supersaturation and corresponding cloud droplet number in a series of simplified offline calculations. The maximum supersaturation and CDN calculated using the parameterization are compared to the full parcel model results in Figure 12, and summarized in Table 2. For the California case studies, the parameterization calculations determine a slightly higher maximum supersaturation, which results in a slightly larger number of cloud droplets activating. There are a number of factors that contribute to this difference. First, slight differences in the value of the enthalpy of phase change of water, and thermal conductivity lead to slightly different moist adiabats. Second, the simplified shape of the Köhler curves and supersaturation profile assumed by the parameterization to obtain a closed solution for the condensation integral (at the point of maximum supersaturation in the cloudy updraft) leads to slightly different growth rates of the droplet distribution. Third, the parameterization uses the temperature, pressure, and vertical velocity at the cloud base to approximate their values at the maximum supersaturation level, but it does not take into account how these evolve as the parcel travels upward in the cloud. Finally, any droplet reduction through the "deactivation" mechanism of *Nenes et al.* [2001] above the point of maximum supersaturation is not accounted for by the parameterization, and may (under conditions of very high CCN) lead to some overprediction in droplet number

compared to the parcel model. Overall however, the evaluation here suggests that the parameterization captures droplet number well.

7. Conclusion

[35] We have used a chemically detailed microphysical parcel model to quantify activation of BC-type particles to cloud droplets in California. The aerosol particles are modeled as external mixtures of internally mixed chemical components constrained by observations at five field sites that are representative of different regions in California. We have assessed one aspect of GCM predictions of the aerosol indirect effect of BC mitigation (namely their representation of the cloud albedo effect) by comparing their CDN predictions to the detailed chemical simulations of changing BC concentration on the cloud droplets. The chemically detailed particle distributions from field campaigns were very comparable to the emission inventory-based particle concentrations used in GCMs. The particle number size distributions agree well for the three models. BC particles in the parcel model are smaller than the GCMs possibly because the locations and seasons of the field campaigns did not represent all of the particle sources included in the GCMs.

[36] The parcel model simulated a simple cloud layer that was consistent with typical stratocumulus observations, while incorporating accurate kinetic activation of chemically resolved particle distributions to cloud droplets. In the polluted California environment, BC-type particles contribute between 14% and 18% of the total cloud droplets. The CDN concentrations from the chemically detailed microphysical calculation agree reasonably well with GCM predictions for California. The parcel model predicted that BC mitigation reduces the droplet population in clouds by between 5% and 9%, with a corresponding increase in mean droplet size. This result agrees well with predictions for the half fossil fuel case from the *Chen et al.* [2010b] model (with a smaller relative magnitude). The predicted decrease in CDN by these two models differs from the *Jacobson* [2010] model which found that fossil soot mitigation (in isolation from biomass burning soot) caused a 1% increase in CDN concentration. This difference was likely the result of that model's treatment of fossil fuel BC particles as initially hydrophobic, although its inclusion of semi-direct and cloud absorption feedbacks could have also reduced CDN by reducing cloud supersaturation.

[37] The reduction in CDN in California due to the decrease in activated BC particles supports the concern raised by *Chen et al.* [2010a] that the cloud albedo effect of BC particles partially offsets the direct forcing reduction. This effect was in fact also evident in the *Jacobson* [2010] results when the larger number of more hygroscopic biomass burning particles was removed and CDN decreased by 10%. This result suggests that for regions like the California sites studied here, where BC mitigation targets fossil fuel sources, a critical aspect of the modeled reduction is the hygroscopicity of the BC particles removed as well as their relative contribution to particle concentrations. Nonetheless, a complete understanding of the BC mitigation in California and the rest of the world (including processes such as the impact on sea ice and land glaciers) requires further work to better constrain the other effects of BC on climate.

References

Adams, P. J., and J. H. Seinfeld (2002), Predicting global aerosol size distributions in general circulation models, *J. Geophys. Res.*, *107*(D19), 4370, doi:10.1029/2001JD001010.

Allen, J. O., et al. (2000), Particle detection efficiencies of aerosol time of flight mass spectrometers under ambient sampling conditions, *Environ. Sci. Technol.*, *34*(1), 211–217, doi:10.1021/es9904179.

Andreae, M. O., and P. Merlet (2001), Emission of trace gases and aerosols from biomass burning, *Global Biogeochem. Cycles*, *15*(4), 955–966, doi:10.1029/2000GB001382.

Andreae, M. O., and D. Rosenfeld (2008), Aerosol-cloud-precipitation interactions. Part 1. The nature and sources of cloud-active aerosols, *Earth Sci. Rev.*, *89*(1–2), 13–41, doi:10.1016/j.earscirev.2008.03.001.

Ault, A. P., et al. (2009), Impact of emissions from the Los Angeles port region on San Diego air quality during regional transport events, *Environ. Sci. Technol.*, *43*(10), 3500–3506, doi:10.1021/es8018918.

Bahadur, R., et al. (2010), Composition and morphology of individual combustion, biomass burning, and secondary organic particle types obtained using urban and coastal ATOFMS and STXM-NEXAFS measurements, *Aerosol Sci. Technol.*, *44*(7), 551–562, doi:10.1080/02786821003786048.

Bahadur, R., et al. (2011), Impact of California's air pollution laws on black carbon and their implications for direct radiative forcing, *Atmos. Environ.*, *45*(5), 1162–1167, doi:10.1016/j.atmosenv.2010.10.054.

Bauer, S. E., et al. (2010), A global modeling study on carbonaceous aerosol microphysical characteristics and radiative effects, *Atmos. Chem. Phys.*, *10*(15), 7439–7456, doi:10.5194/acp-10-7439-2010.

Bhave, P. V., et al. (2002), A field-based approach for determining ATOFMS instrument sensitivities to ammonium and nitrate, *Environ. Sci. Technol.*, *36*(22), 4868–4879, doi:10.1021/es015823i.

Bond, T. C., E. Bhardwaj, R. Dong, R. Jogani, S. Jung, C. Roden, D. G. Streets, and N. M. Trautmann (2007), Historical emissions of black and organic carbon aerosol from energy-related combustion, 1850–2000, *Global Biogeochem. Cycles*, *21*, GB2018, doi:10.1029/2006GB002840.

Cantrell, W., G. Shaw, and R. Benner (1999), Cloud properties inferred from bimodal aerosol number distributions, *J. Geophys. Res.*, *104*(D22), 27,615–27,624, doi:10.1029/1999JD900252.

Chen, W.-T., Y. H. Lee, P. J. Adams, A. Nenes, and J. H. Seinfeld (2010a), Will black carbon mitigation dampen aerosol indirect forcing?, *Geophys. Res. Lett.*, *37*, L09801, doi:10.1029/2010GL042886.

Chen, W.-T., A. Nenes, H. Liao, P. J. Adams, J.-L. F. Li, and J. H. Seinfeld (2010b), Global climate response to anthropogenic aerosol indirect effects: Present day and year 2100, *J. Geophys. Res.*, *115*, D12207, doi:10.1029/2008JD011619.

Durkee, P. A., et al. (2000), The Monterey Area Ship Track experiment, *J. Atmos. Sci.*, *57*(16), 2523–2541, doi:10.1175/1520-0469(2000)057<2523:TMASTE>2.0.CO;2.

Dusek, U., et al. (2006), CCN activation of pure and coated carbon black particles, *Environ. Sci. Technol.*, *40*(4), 1223–1230, doi:10.1021/es0503478.

Emanuel, K. A., and M. Bister (1996), Moist convective velocity and buoyancy scales, *J. Atmos. Sci.*, *53*(22), 3276–3285, doi:10.1175/1520-0469(1996)053<3276:MCVABS>2.0.CO;2.

Erlick, C., L. M. Russell, and V. Ramaswamy (2001), A microphysics-based investigation of the radiative effects of aerosol-cloud interactions for two MAST Experiment case studies, *J. Geophys. Res.*, *106*(D1), 1249–1269, doi:10.1029/2000JD900567.

Forster, P. et al. (2007), Changes in atmospheric constituents and in radiative forcing, in *Climate Change 2007: The Physical Science Basis. Contribution of Working Group I to the Fourth Assessment Report of the Intergovernmental Panel on Climate Change*, edited by S. Solomon et al., pp. 129–234, Cambridge Univ. Press, Cambridge, U. K.

Fountoukis, C., and A. Nenes (2005), Continued development of a cloud droplet formation parameterization for global climate models, *J. Geophys. Res.*, *110*, D11212, doi:10.1029/2004JD005591.

Ghan, S. J. (2011), Droplet nucleation: Physically based parameterizations and comparative evaluation, *J. Adv. Model. Earth Syst.*, *3*, M10001, doi:10.1029/2011MS000074.

Guibert, S., J. R. Snider, and J.-L. Brenguier (2003), Aerosol activation in marine stratocumulus clouds: 1. Measurement validation for a closure study, *J. Geophys. Res.*, *108*(D15), 8628, doi:10.1029/2002JD002678.

Hansen, J., et al. (1997), The missing climate forcing, *Philos. Trans. R. Soc. B*, *352*(1350), 231–240.

Holecek, J. C., et al. (2005), Single particle chemical analysis of aerosols generated from rain water collected at Trinidad Head, CA during the cloud indirect effects experiment (CIFEX), *Abstr. Pap. Am. Chem. Soc.*, *229*, U127-U.

Jacobson, M. Z. (2002), Control of fossil-fuel particulate black carbon and organic matter, possibly the most effective method of slowing global warming, *J. Geophys. Res.*, *107*(D19), 4410, doi:10.1029/2001JD001376.

Jacobson, M. Z. (2006), Effects of externally through-internally mixed soot inclusions within clouds and precipitation on global climate, *J. Phys. Chem. A*, *110*(21), 6860–6873, doi:10.1021/jp056391r.

Jacobson, M. Z. (2010), Short-term effects of controlling fossil-fuel soot, biofuel soot and gases, and methane on climate, Arctic ice, and air pollution health, *J. Geophys. Res.*, *115*, D14209, doi:10.1029/2009JD013795.

Koch, D., and A. D. Del Genio (2010), Black carbon semi-direct effects on cloud cover: Review and synthesis, *Atmos. Chem. Phys.*, *10*(16), 7685–7696, doi:10.5194/acp-10-7685-2010.

Koch, D., et al. (2009), Distinguishing aerosol impacts on climate over the past century, *J. Clim.*, *22*(10), 2659–2677, doi:10.1175/2008JCLI2573.1.

Koch, D., et al. (2011), Soot microphysical effects on liquid clouds, a multi-model investigation, *Atmos. Chem. Phys.*, *11*(3), 1051–1064, doi:10.5194/acp-11-1051-2011.

Koehler, K. A., et al. (2009), Cloud condensation nuclei and ice nucleation activity of hydrophobic and hydrophilic soot particles, *Phys. Chem. Chem. Phys.*, *11*(36), 7906–7920, doi:10.1039/b905334b.

Kristjansson, J. E., T. Iversen, A. Kirkevåg, Ø. Seland, and J. Debernard (2005), Response of the climate system to aerosol direct and indirect forcing: Role of cloud feedbacks, *J. Geophys. Res.*, *110*, D24206, doi:10.1029/2005JD006299.

Lammel, G., and T. Novakov (1995), Water nucleation properties of carbon black and diesel soot particles, *Atmos. Environ.*, *29*(7), 813–823, doi:10.1016/1352-2310(94)00308-8.

Lohmann, U., and J. Feichter (2005), Global indirect aerosol effects: A review, *Atmos. Chem. Phys.*, *5*, 715–737, doi:10.5194/acp-5-715-2005.

Lu, M. L., W. C. Conant, H. H. Jonsson, V. Varutbangkul, R. C. Flagan, and J. H. Seinfeld (2007), The Marine Stratus/Stratocumulus Experiment (MASE): Aerosol-cloud relationships in marine stratocumulus, *J. Geophys. Res.*, *112*, D10209, doi:10.1029/2006JD007985.

Lucas, C., et al. (1994), Convective available potential-energy in the environment of oceanic and continental clouds—Correction and comments, *J. Atmos. Sci.*, *51*(24), 3829–3830, doi:10.1175/1520-0469(1994)051<3829:CAPEIT>2.0.CO;2.

Meskhidze, N., A. Nenes, W. C. Conant, and J. H. Seinfeld (2005), Evaluation of a new cloud droplet activation parameterization with in situ data from CRYSTAL-FACE and CSTRIPE, *J. Geophys. Res.*, *110*, D16202, doi:10.1029/2004JD005703.

Moffet, R. C., et al. (2008), Measurement of ambient aerosols in northern Mexico City by single particle mass spectrometry, *Atmos. Chem. Phys.*, *8*(16), 4499–4516, doi:10.5194/acp-8-4499-2008.

Morales, R., and A. Nenes (2010), Characteristic updrafts for computing distribution-averaged cloud droplet number and stratocumulus cloud properties, *J. Geophys. Res.*, *115*, D18220, doi:10.1029/2009JD013233.

Nenes, A., and J. H. Seinfeld (2003), Parameterization of cloud droplet formation in global climate models, *J. Geophys. Res.*, *108*(D14), 4415, doi:10.1029/2002JD002911.

Nenes, A., et al. (2001), Kinetic limitations on cloud droplet formation and impact on cloud albedo, *Tellus, Ser. B*, *53*(2), 133–149, doi:10.1034/j.1600-0889.2001.d01-12.x.

Nicholls, S., and J. Leighton (1986), An observational study of the structure of stratiform cloud sheets. 1. Structure, *Q. J. R. Meteorol. Soc.*, *112*(472), 431–460, doi:10.1002/qj.49711247209.

Ogren, J. A., and R. J. Charlson (1983), Elemental carbon in the atmosphere—Cycle and lifetime, *Tellus, Ser. B*, *35*(4), 241–254, doi:10.1111/j.1600-0889.1983.tb00027.x.

Pratt, K. A., et al. (2010), In situ chemical characterization of aged biomass-burning aerosols impacting cold wave clouds, *J. Atmos. Sci.*, *67*(8), 2451–2468, doi:10.1175/2010JAS3330.1.

Pruppacher, H. R., and J. D. Klett (2003), *Microphysics of Clouds and Precipitation*, Kluwer Acad., Norwell, Mass.

Qin, X. Y., et al. (2006), Comparison of two methods for obtaining quantitative mass concentrations from aerosol time-of-flight mass spectrometry measurements, *Anal. Chem.*, *78*(17), 6169–6178, doi:10.1021/ac060395q.

Ramanathan, V., and G. Carmichael (2008), Global and regional climate changes due to black carbon, *Nat. Geosci.*, *1*(4), 221–227, doi:10.1038/ngeo156.

Roberts, G. C., A. Nenes, J. H. Seinfeld, and M. O. Andreae (2003), Impact of biomass burning on cloud properties in the Amazon Basin, *J. Geophys. Res.*, *108*(D2), 4062, doi:10.1029/2001JD000985.

Russell, L. M., and J. H. Seinfeld (1998), Size- and composition-resolved externally mixed aerosol model, *Aerosol Sci. Technol.*, *28*(5), 403–416, doi:10.1080/02786829808965534.

Russell, L. M., et al. (1999), Aerosol dynamics in ship tracks, *J. Geophys. Res.*, *104*(D24), 31,077–31,095, doi:10.1029/1999JD900985.

Russell, L. M., et al. (2011), Identifying organic aerosol sources by comparing functional group composition in chamber and atmospheric particles, *Proc. Natl. Acad. Sci. U. S. A.*, *108*(9), 3516–3521, doi:10.1073/pnas.1006461108.

Shields, L. G., et al. (2008), Detection of ambient ultrafine aerosols by single particle techniques during the SOAR 2005 campaign, *Aerosol Sci. Technol.*, *42*(8), 674–684, doi:10.1080/02786820802227378.

Silva, P. J., and K. A. Prather (1997), On-line characterization of individual particles from automobile emissions, *Environ. Sci. Technol.*, *31*(11), 3074–3080, doi:10.1021/es961063d.

Silva, P. J., et al. (1999), Size and chemical characterization of individual particles resulting from biomass burning of local Southern California species, *Environ. Sci. Technol.*, *33*(18), 3068–3076, doi:10.1021/es980544p.

Snider, J. R., S. Guibert, J.-L. Brenguier, and J.-P. Putaud (2003), Aerosol activation in marine stratocumulus clouds: 2. Köhler and parcel theory closure studies, *J. Geophys. Res.*, *108*(D15), 8629, doi:10.1029/2002JD002692.

Sodeman, D. A., et al. (2005), Determination of single particle mass spectral signatures from light-duty vehicle emissions, *Environ. Sci. Technol.*, *39*(12), 4569–4580, doi:10.1021/es0489947.

Spracklen, D. V., et al. (2011), Global cloud condensation nuclei influenced by carbonaceous combustion aerosol, *Atmos. Chem. Phys.*, *11*(17), 9067–9087, doi:10.5194/acp-11-9067-2011.

Stier, P., et al. (2007), Aerosol absorption and radiative forcing, *Atmos. Chem. Phys.*, *7*(19), 5237–5261, doi:10.5194/acp-7-5237-2007.

Suess, D. T., and K. A. Prather (1999), Mass spectrometry of aerosols, *Chem. Rev.*, *99*(10), 3007–3036, doi:10.1021/cr980138o.

Yan, F., et al. (2011), Global emission projections of particulate matter (PM): I. Exhaust emissions from on-road vehicles, *Atmos. Environ.*, *45*(28), 4830–4844, doi:10.1016/j.atmosenv.2011.06.018.